

Molecular Gas and Star-Formation In Low Surface Brightness Galaxies

Tian-Wen Cao^{1,2,3}, Hong Wu*^{1,2}, Wei Du¹, Feng-Jie Lei^{1,2}, Ming Zhu¹, Jan Wouterloot⁴, Harriet Parsons⁴, Yi-Nan Zhu¹, Chao-Jian Wu¹, Fan Yang¹, Chen Cao⁵, Zhi-Min Zhou¹, Min He^{1,2}, Jun-Jie Jin^{1,2}, James E. Wicker¹

ABSTRACT

We have obtained CO(J=2-1) spectra of nine face-on low surface brightness galaxies (LSBGs) using the JCMT 15-meter telescope and observed $H\alpha$ images using the 2.16-meter telescope of NAOC. As no CO has been detected, only upper limits on the H_2 masses are given. The upper limits of total molecular hydrogen masses are about $(1.2-82.4) \times 10^7 M_\odot$. Their star formation rates are mainly lower than $0.4 M_\odot \text{ yr}^{-1}$ and star formation efficiencies are lower than $1.364 \times 10^{-10} \text{ yr}^{-1}$. Our results show that the absence of molecular gas content is the direct reason for the low star formation rate. The low star formation efficiency probably resulted from the low efficiency of HI gas transforming to H_2 gas.

Subject headings: galaxies: molecules — galaxies: evolution — galaxies: star formation rate

¹Key Laboratory of Optical Astronomy, National Astronomical Observatories, Chinese Academy of Sciences, Beijing 100012, P.R. China; twcao@bao.ac.cn

²School of Astronomy and Space Science, University of Chinese Academy of Sciences, Beijing, P.R. China; hwu@bao.ac.cn

³Chinese Academy of Sciences South America Center for Astronomy, China-Chile Joint Center for Astronomy, Camino El Observatorio 1515, Las Condes, Santiago, Chile

⁴East Asian Observatory, 660 N. Aohōkū Place, University Park, Hilo, Hawaii 96720, USA

⁵School of Space Science and Physics, Shandong University at Weihai, Weihai, Shandong 264209, China

1. Introduction

Low Surface Brightness galaxies (LSBGs, Impey & Bothun (1997)) are important for investigating the evolution of our universe. The origin and evolution of these LSBGs are still mysterious. They have significantly different chemical enrichment histories from normal galaxies (Peebles 2001; Pustilnik et al. 2011). LSBGs are usually optically faint and blue (de Blok et al. 1995; Impey & Bothun 1997). The stellar disks of most LSBGs are diffuse. They usually have low metallicities ($Z < 1/3 Z_{\odot}$ McGaugh (1994)), low column densities ($N_{HI} \sim 10^{20} \text{ cm}^{-2}$ de Blok et al. (1996)) and low dust masses (Matthews & Wood 2001). The star formation rates (SFRs) of LSBGs are lower than those of normal galaxies (Gerritsen & de Blok 1999; Boissier et al. 2008; Wyder et al. 2009).

According to previous works, the HI content of most LSBGs is rich, compared with normal star-forming galaxies (McGaugh 1994). The HI gas disk extends well beyond the stellar disk (McGaugh & de Blok 1997; Gerritsen & de Blok 1999; O’Neil et al. 2004; Matthews et al. 2001), and is about double the size of the optical disk (de Blok et al. 1996; Pickering et al. 1997; Das et al. 2007).

Although the original material involved in star formation is HI, the star formation is indirectly related with HI. Generally, the star formation arises out of molecular clouds. The low star formation rates in LSBGs may be related to the absence of molecular gas content. The optical peculiarities of LSBGs have been discussed by some works (van der Hulst et al. 1993; McGaugh & Bothun 1994; McGaugh 1994; de Blok et al. 1995; Impey & Bothun 1997; Jimenez et al. 1998), however, the cold molecular gas in these galaxies is far from well understood. Molecular gas is vital for studying the star formation process. There are some previous works which try to detect the CO content in LSBGs (Schombert et al. 1990; Knezek 1993; de Blok & van der Hulst 1998b; Braine et al. 2000). Most works just give upper limits on CO content, and only a few LSBGs have detected molecular gas (Matthews & Gao 2001; O’Neil et al. 2003; Matthews et al. 2005; Das et al. 2010; Haynes et al. 2011). This may indicate a shortage of molecular gas in LSBGs.

To explore the low star formation efficiency of LSBGs, we need to know which phase is dominant during star formation. There are two phases in formation of a star: Firstly, the HI gas transforms into molecular gas, then molecular gas forms

a star. The CO(J=2-1) emission line is used to trace molecular hydrogen gas in this work. We observe the CO(J=2-1) emission line by JCMT, H α images by the 2.16-meter telescope of NAOC and also combine with NUV data from GALEX and HI data from Arecibo.

In this paper, the sample and observations of LSBGs are presented in §2. Results and analysis are given in §3. Discussion and summary are provided in §4 and §5.

2. The Sample and Observation of LSBGs

2.1. Sample

The Arecibo Legacy Fast ALFA (ALFALFA) survey (Giovanelli et al. 2005), which covers 7000 deg² of high Galactic latitude sky, provides a 21-cm HI emission line spectral database with redshift from 1600 to 18000 kms⁻¹ and velocity resolution of 5 kms⁻¹. The α .40 catalog is the first released catalog, which covers 40% of the area of the ALFALFA survey and contains 15855 objects (Haynes et al. 2011). About 78% sources have optical counterparts from the Sloan Digital Sky Survey (SDSS, Haynes et al. (2011)).

Based on the α .40 catalog, Du et al. (2015) selects a sample of LSBGs which contains 1129 LSBGs with surface brightness $\mu_{B(0)obs}$ larger than 22.5 mag/arcsec². We selected nine LSBGs from this sample. They all have face-on disks and their HI masses are about $(0.52-19.9) \times 10^9 M_{\odot}$, which are expected to have higher fluxes of CO(J=2-1) emission lines than others in the 1129 LSBGs sample. The redshifts in our sample are between 0.0029 and 0.0339. Generally, the size of the CO disk is about half the size of the optical disk (Young & Knezek 1989) and the optical sizes of nine targets are about 30-80 arcseconds. Figure 1 shows r-band images of our nine LSBGs from SDSS DR12. More details about properties of the galaxies are shown in Table 1.

2.2. CO(J=2-1) emission

We obtained CO(J=2-1) spectra of nine targets using the R×A3 receiver with ACSIS as the backend, mounted on the JCMT 15-meter telescope near the peak of Mauna Kea, Hawaii. The half power beam width (HPBW) is about 20'' at 230 GHz. The frequency coverage of the A3 receiver ranges from 211.5 to 276.5 GHz and the CO(J=2-1) spectra of our objects shift from 222.99 to 229.86 GHz. The A3 receiver gives 1936 channels over a bandwidth of 1 GHz with a channel separation of 0.516 MHz, and the velocity resolution is 0.674 km/s (one channel).

The targets are finally observed under band 4 weather⁶ in March and band 5 weather in August of 2015. In band 4 weather the atmospheric zenith opacity at 225 GHz, as measured with the Water Vapour Monitor (measured in the direction in which the telescope is observing), or the CSO tau meter (measuring in a fixed direction), is between 0.12 and 0.20. In band 5 weather the zenith opacity is between 0.20 and 0.32. The on-source integration time per scan was 400 seconds and one such scan took 13 minutes. The observation mode was 'double beam switching'⁷ over 60 arcseconds(to both sides with respect to the source). The total integration time of each object is about two hours and eight hours for band 4 weather and band 5 weather, respectively. The data are calibrated by ORAC-DR(Hirst & Cavanagh 2005) data-reduction pipeline⁸ using STARLINK software. In Table 2, columns 2-6 show details about the observations of CO(J=2-1) emission line.

2.3. H α Images

The H α images of NGC7589 and AGC Nr12212 have been observed by van Zee (2000), Epinat et al. (2008) and Subramanian et al. (2016). The H α images of other seven LSBGs were observed by the 2.16-meter telescope at Xinglong Observatory, administered by the National Astronomical Observatories, Chinese Academy of Sciences (NAOC). This facility houses the BAO Faint Object Spectrograph and Camera

⁶<http://www.eaobservatory.org/jcmt/observing/weather-bands/>

⁷<http://www.eaobservatory.org/jcmt/instrumentation/heterodyne/observing-modes/>

⁸<http://starlink.eao.hawaii.edu/devdocs/sun260.htx/sun260.html>

(BFOSC)(Fan et al. 2016) with a 1272×1152 E2V CCD. The field of view is about 9.46 arcmin × 8.77 arcmin. The pixel size is 0.475 " and the gain is 1.08 e/ADU. Each target was observed with a broad band R filter and one narrow band H α filter. The center wavelength of the R-band filter is 6407 Å and the FWHM is 1580 Å. According to the different redshifts of objects, we employed H α filters with different central wavelength of 6660 Å, 6710 Å and 6760 Å and FWHM of 70 Å. The exposure times are about 600 seconds and 1800 seconds for the R-band and H α narrow bands, respectively.

The image reduction is performed by using IRAF software and the sky background subtraction applied the more accurate method by Zheng et al. (1999), Wu et al. (2002) and Du et al. (2015). The stellar continuum of each Ha image is removed by subtracting scaled R-band image. Finally we measured the Ha fluxes of these LS-BGs, using the ellipse photometry of IRAF. In Table 2, columns 7-10 list the details of observations of H α images. AGCnr102981 is affected by light pollution from a nearby bright star.

3. Results and Analysis

3.1. H_2 Masses

To enhance signal-to-noise, we binned the CO(J=2-1) spectral channels. The final CO(J=2-1) spectral have been smoothed to 15 km/s as shown in Figure 2. Apparently, None of nine targets are detected CO(J=2-1) content.

To estimate the molecular hydrogen masses, we adopted W_{50} as the linewidth. Here, W_{50} is the Full Width at Half Maximum(FWHM) of HI emission line. The W_{50} of our targets is about 65-345 km/s. The aperture efficiency η_a is 0.61 at 225 GHz, and the conversion from T_A in Kelvin to flux density in Jansky is $S(\text{Jy}) = 15.6 \times T_A(\text{K})/\eta_a$, for JCMT. In this work, the T_A is replaced by the $3\sigma/\sqrt{n}$, where the σ is the rms noise at native resolution and n is the number of channels to smooth velocity resolution to 15 km/s. Hence, flux densities in Jansky are calculated according to equation: $S_{CO(J=2-1)}(\text{Jy}) = 15.6 \times 3 \times \sigma/\sqrt{n}/\eta_a$. Here we adopt the $R_{21}=\text{CO}(J=2-1)/\text{CO}(J=1-0)=0.7$ (Leroy et al. 2009; Schruba et al. 2012);

The CO-to-H₂ conversion equation is as follows:

$$M_{H_2} = \alpha_{CO} \times L_{CO} \quad (1)$$

$$L_{CO} = 3.25 \times 10^7 \times S'_{CO} \times \nu_{obs}^{-2} \times D^2 \times (1+z)^{-3} \quad (2)$$

In Equation(1), M_{H_2} is molecular hydrogen mass in M_\odot and L_{CO} is CO luminosity in $K \text{ km s}^{-1} \text{ pc}^2$. In Equation(2), S'_{CO} is integrated CO flux density in Jy km s^{-1} . We adopt linewidth W_{50} and the resolution 15 km/s, Such $S'_{CO(J=1-0)} = S_{CO(J=1-0)} \times W_{50}/15$. ν_{obs} is observation frequency in GHz, D is distance in Mpc and z is redshift.

In different environments, the X_{CO} factor is different. Considering that the conversion factor of CO-to-H₂ increases with decreasing metallicity, X_{CO} is chosen to be $3.162 \times 10^{20} \text{ cm}^{-2}/(\text{K km s}^{-1})$ ($X_{CO} = \alpha_{CO} \times 6.3 \times 10^{19} \text{ pc}^2 \text{ cm}^{-2} M_\odot^{-1}$, α_{CO} simply is a mass-to-light ratio in $M_\odot(\text{K km s}^{-1} \text{ pc}^2)^{-1}$ Bolatto et al. (2013)) which is also the same as previous works(Matthews & Gao 2001; Matthews et al. 2005). From Equation (1), we can calculate upper limits of molecular hydrogen masses per beam, which are about $(0.68\text{-}31.6) \times 10^7 M_\odot$.

To compare with previous works, we correct the beam size to the CO disk size of our LSBGs. We estimate the upper limits of total molecular hydrogen masses of our sample. The beam filling factors are defined as the ratios between the area of beam and the total area of CO disk which is generally half of the optical disk(Young & Knezek 1989), and listed in Table 3. The major-axis of optical disks are given by R band images and listed in the Table 1. The size of NGC7589 is from Lauberts & Valentijn (1989). The upper limits of total molecular hydrogen masses are about $(1.2\text{-}82.4) \times 10^7 M_\odot$ which are listed in Table 3. Since the HI disk is more extended in LSBGs, the CO disk may be larger than half of optical disk. The total molecular hydrogen masses may be underestimated in Table 3. In the following parts of this paper, M_{H_2} represents the total molecular hydrogen mass.

In Figure 3, we plot the M_{HI} versus M_{H_2} including our sample and LSBGs from some previous works. We have calculated the average molecular mass with bin size in $10^{0.5} M_\odot$. The average of M_{H_2} of LSBGs is smaller than those in star forming (SF) galaxies for a given HI mass. We can see that upper limits of M_{H_2} in our work are consistent with previous works. LSBGs are deficient of the molecular gas compared with these SF galaxies.

32 nearby gas-rich SF galaxies in Figure 3 are from Jiang et al. (2015) and observed with the Sub-millimeter Telescope (SMT). Their HI masses are from the ALFALFA catalog. These SF galaxies are intermediate-mass galaxies ($<10^{10} M_{\odot}$). The intermediate-mass galaxies were found to be more gas rich (Blanton & Moustakas 2009). These galaxies present the low-mass end of main sequence star-forming galaxies. Both the molecular mass of our sample and SF galaxies sample are calculated by the CO(J=2-1) emission line, so the SF galaxies are selected as a comparison sample.

Some reasons could explain the lack of molecular gas in LSBGs. Firstly, metallicity can affect the cooling efficiency of the Interstellar Medium (ISM) which may impact the formation of Giant Molecular Clouds (GMCs). Secondly, dust grains where H_2 forms (Savage & Mathis 1979) can shield molecular gas from photodissociation. The low interstellar medium (ISM) densities make it hard for molecular clouds to form and be maintained.

The low metallicities and low ISM densities in LSBGs can make it either difficult to form H_2 or easy to destroy H_2 .

3.2. Star Formation Rates

We adopt $H\alpha$ luminosity to calculate SFR of our sample. As the dust in LSBGs is usually less, few targets can be detected in 22 μm (WISE W4) band, so we ignore the dust extinction in our sample.

The SFR of AGCNR12212 has been found to be $0.111 M_{\odot}\text{yr}^{-1}$ in the work of van Zee (2000) and $0.056 M_{\odot}\text{yr}^{-1}$ in the work of Epinat et al. (2008). Six $H\alpha$ fluxes of LSBGs are available from our observation. We transform $H\alpha$ fluxes to luminosity using the relation: $L = 4 \times \pi \times D^2 \times F$, where D is distance in centimeter and F is $H\alpha$ flux in erg/s/cm^2 . We employ the following equation to calculate SFR(Kennicutt 1998):

$$\text{SFR}_{H\alpha}(M_{\odot}\text{yr}^{-1}) = 7.9 \times 10^{-42} \times L_{H\alpha} \text{ erg/s} \quad (3)$$

The derived SFRs are from 0.056 to $0.829 M_{\odot}\text{yr}^{-1}$.

We also use the NUV-band luminosity to calculate SFR of four sources (AGCNR4528, 110150, 102635, NGC 7589) which have NUV data from GALEX. We adopt the fol-

lowing equation (Kennicutt 1998):

$$\text{SFR}_{UV}(\text{M}_{\odot}\text{yr}^{-1}) = 1.4 \times 10^{-28} \times L_{\nu}(\text{erg/s/Hz}) \quad (4)$$

The NUV-based SFRs are $0.146\sim 1.003 \text{ M}_{\odot}\text{yr}^{-1}$, which are systematically larger than those calculated from $\text{H}\alpha$ luminosity. The UV emission is also contaminated by older stars, so this would lead to deriving higher SFR from UV than that from the $\text{H}\alpha$. All these values are listed in the Table 3.

In Figure 5, we show SFR versus HI mass for our sample and black lines connect the same target. We also show another sample of LSBGs in green dots from Boissier et al. (2008) whose SFRs are estimated by NUV luminosity. The Figure shows an increase of the SFR with HI mass. SFR in LSBGs is about $0.2 \text{ M}_{\odot}\text{yr}^{-1}$ in the model calculations of McGaugh & Bothun (1994) and $0.17\text{-}0.36 \text{ M}_{\odot}\text{yr}^{-1}$ by $\text{H}\alpha$ (Burkholder et al. 2001), they are lower than that of SF galaxies. The low SFRs of our sample are consistent with previous results. The low SFR in LSBGs agrees with the low molecular hydrogen mass.

3.3. Star Formation Efficiency

Star formation efficiency (SFE) (Leroy et al. 2008) is the ratio of star formation rate to total mass of gas ($\text{SFE} = \text{SFR} / \text{M}_{gas}$). M_{gas} is the total gas mass which can be estimated by H_2 mass and HI mass ($\text{M}_{H_2} + \text{M}_{HI}$).

The SFR and M_{H_2} of our sample have been calculated in §3.1 and §3.2. M_{HI} is from the ALFALFA catalog listed in Table 2. Since M_{H_2} is far smaller than M_{HI} , we adopt M_{HI} to replace M_{gas} . SFE can be calculated by $\text{SFR}_{H\alpha}$ and SFR_{UV} , respectively. SFEs of our LSBGs are $(0.165\sim 1.364) \times 10^{-10} \text{ yr}^{-1}$ by $\text{SFR}_{H\alpha}$ and $(0.471\sim 1.174) \times 10^{-10} \text{ yr}^{-1}$ by SFR_{UV} , respectively. The results are shown in Table 3.

SFEs of LSBGs are lower than $1.364 \times 10^{-10} \text{ yr}^{-1}$ and are far lower than $5.25 \times 10^{-10} \text{ yr}^{-1}$ observed in normal spiral galaxies (Leroy et al. 2008). Generally, molecular gas is directly related to star formation, so SFE can reflect the efficiency of transforming hydrogen atom to molecular hydrogen. Low SFE may hint that atomic hydrogen produces molecular hydrogen at a low speed. In short, the low SFR and

SFE imply a lack of molecular hydrogen gas in LSBGs and this will be discussed in §4.

4. Discussion

4.1. Comment of Individual Galaxies

AGC Nr12289: is a late-type spiral galaxy with a optical disk size of about $35''$ and has a potential AGN/LINER core (Schombert 1998). There is a supernova (SN2002en) in AGC Nr12289. O’Neil et al. (2003) has detected CO(J=1-0,J=2-1) content in AGC Nr12289 using the IRAM 30-meter telescope. The M_{H_2} of AGC Nr12289 is about $15.8 \times 10^7 M_\odot$ using CO(J=2-1) observed by IRAM, which is lower than our upper limit of $41.2 \times 10^7 M_\odot$. The ratio of M_{H_2}/M_{HI} is 0.008 for AGC Nr12289.

AGC Nr188845, AGC Nr102243, AGC Nr102635, AGC Nr102981: For these galaxies, the optical sizes are about $54''$, $52''$, $46''$ and $46''$. From our calculations, the M_{H_2}/M_{HI} are lower than 0.044, 0.017, 0.048 and 0.018, respectively. The metallicity of AGC Nr188845 is 0.01 and 1/2 of solar metallicity. AGC Nr102981 is a typical late-type spiral galaxy and the spiral structures are shown in Figure 1.

AGC Nr4528, AGC Nr12212, AGC Nr110150: The optical sizes of these three galaxies are about $66''$, $62''$ and $80''$ respectively which indicate that JCMT’s beam size is not enough to cover their total CO content. The metallicity of AGC Nr4528 is 0.02 and same to solar metallicity. The M_{H_2}/M_{HI} for these three LSBGs are lower than 0.018, 0.0201 and 0.022 respectively.

NGC 7589: The optical size of NGC 7589 is $76''$. It is a Seyfert-1 galaxy. The SFR from NUV band is $1.003 M_\odot \text{yr}^{-1}$ and its metallicity is 0.04 and twice the solar metallicity. There are some works investigating this galaxy. It is a typical giant LSBG and has type 1 XUV-disk galaxy(Boissier et al. 2008). The upper limit of M_{H_2} is $8.25 \times 10^8 M_\odot$ and the ratio of M_{H_2}/M_{HI} is lower than 0.081.

4.2. M_{H_2} Versus $L_{12\mu m}$

The $12\ \mu m$ (WISE W3) band is an effective probe of star formation (Donoso et al. 2012) and has a good linear relationship with molecular hydrogen mass for SF galaxies (Jiang et al. 2015). In this section, we try to explore the relation between molecular gas and $12\ \mu m$ emission in LSBGs.

Five sources in our sample have $12\ \mu m$ emission data provided by the WISE ALL-SKY Survey. Figure 4 shows $L_{12\mu m}$ versus M_{H_2} . The blue line in Figure 4 is the relationship between M_{H_2} ($CO_{J=2-1}$) and luminosity of $12\ \mu m$ for SF galaxies (Jiang et al. 2015).

AGC Nr12289 and NGC 7589 have higher luminosities of $12\ \mu m$ in Figure 4. AGC Nr12289 has a potential AGN/LINER core and NGC 7589 is a Seyfert 1 galaxy which may cause them to be different from other LSBGs in our sample. The LSBGs show low luminosities of $12\ \mu m$ and it may mean less dust in LSBGs. For SF galaxies, they always have larger $12\ \mu m$ luminosities compared with LSBGs.

4.3. The Stellar Mass and Gas Content

Six LSBGs of our sample have $3.4\ \mu m$ (WISE W1) band data. Using the method in Wen et al. (2013) by following Equation (5), we adopt $3.4\ \mu m$ data to calculate the stellar mass:

$$\log_{10}(M_*/M_\odot) = (-0.040 \pm 0.001) + (1.120 \pm 0.001) \times \log_{10}(\nu L_\nu(3.4\ \mu m)/L_\odot) \quad (5)$$

As the redshifts of our sample are small, we ignore the k-correction. Their stellar masses are about $(1.41-83.17) \times 10^8 M_\odot$. LSBGs usually have low masses. The stellar masses of our sample are shown in Table 3.

The stellar masses of SF galaxies have a different relation with molecular gas and atomic gas. The ratios of M_{H_2}/M_* are almost constant (Jiang et al. 2015). We are more interested in the relation between stellar mass and gas content of LSBGs.

Figure 6 shows the relation between stellar mass M_* and gas content in SF galaxies and our LSBG sample. The M_{H_2}/M_* shows a flat trend within the considerable scatter and M_{HI}/M_* shows an obvious decline with increasing stellar mass. It seems

that the molecular gas fraction (M_{H_2}/M_*) is similar in LSBGs and in SF galaxies, although our results just provide upper limits except for the AGC Nr12289. Compared with SF galaxies, the stellar mass of our sample is mainly lower than $10^9 M_\odot$ excluding the two special galaxies (AGC Nr12289 and NGC7589). Stellar masses of AGC Nr12289 and NGC7589 may be overestimated by the central AGN.

4.4. M_{H_2}/M_{HI} and SFR/M_{H_2}

HI gas is the original material involved in star formation, and star formation is directly related to molecular gas. The M_{H_2}/M_{HI} ratio should be different for different galaxies. The gas content could change along the Main-Sequence of star-forming galaxies. Other factors, such as metallicity, environment could affect the ratio. Even for the same galaxy, its gas fraction would also change during its different evolutionary phase. In our nine LSBGs, the M_{H_2}/M_{HI} ratios are less than 0.02. In typically brighter Sd-Sm spirals (Young & Knezek 1989), the M_{H_2}/M_{HI} ratio is about 0.2.

In the section 3.1, we have discussed the M_{HI} and M_{H_2} in SF galaxies and LSBGs. The M_{H_2} in LSBGs is lower than that in SF galaxies. In this section we compare M_{H_2}/M_{HI} and SFR/M_{H_2} in those LSBGs and SF galaxies.

Figure 7 show the distribution of M_{H_2}/M_{HI} on the left and SFR/M_{H_2} on the right. In right panel, NGC7589 has completely different values of SFR/M_{H_2} from the other LSBGs because of AGN influence. Due to the dispersed distribution, the difference in SFR/M_{H_2} between SF galaxies and LSBGs is not quite obvious.

We can see that the ratios of M_{H_2}/M_{HI} in LSBGs are less than those in SF galaxies. The rate of transforming atomic hydrogen to molecular hydrogen in LSBGs is lower than that in SF galaxies. In Section 3.1, we also have discussed the shortage of molecular gas in the special environment of LSBGs. However, CO is more easily photodissociated than H_2 in a metal-poor environment (Wolfire et al. 2010; Shetty et al. 2011). Thus, the conversion factor of CO-to- H_2 is usually higher than that in SF galaxies. In this work, we adopt the factor $3.162 \times 10^{20} \text{ cm}^{-2}/(\text{K kms}^{-1})$ to be consistent with previous works. According to the work of Narayanan et al. (2012), the factor may be larger than $3.16 \times 10^{20} \text{ cm}^{-2}/(\text{K kms}^{-1})$ and up to $15 \times$

$10^{20} \text{ cm}^{-2}/(\text{K kms}^{-1})$. So, the M_{H_2} of our sample may be underestimated. Although lacking a detected CO content, it is still possible that M_{H_2} is underestimated in LSBGs.

5. Summary

We observed CO(J=2-1) emission lines in nine LSBGs with JCMT and $H\alpha$ images with the 2.16-meter telescope administered by NAOC. As no CO has been detected, only upper limits on the H_2 masses are given. The upper limits of hydrogen molecular masses are about $(1.2\text{-}82.4) \times 10^7 M_\odot$. Their star formation rates are about $0.056\text{-}0.83 M_\odot\text{yr}^{-1}$ and $0.146\text{-}1.003 M_\odot\text{yr}^{-1}$ estimated by $H\alpha$ and NUV luminosities, respectively. The stellar masses are about $(0.14\text{-}8.31) \times 10^9 M_\odot$ estimated by the WISE $3.4 \mu\text{m}$ band. From our results, the M_{H_2} and stellar mass in LSBGs are lower than those in SF galaxies. Low SFRs in LSBGs may be related to low molecular hydrogen mass, which may indicate low productivity of atomic hydrogen transforming into molecular hydrogen. More direct detection of molecular gas of LSBG is the key to answer the question in the future.

Acknowledgments

We would like to thank the referee for helpful suggestions. We thank the Key Laboratory of Optical Astronomy and Xinglong Observing Station administered by NAOC for their help during observations. We also thank the ALFALFA team for providing the $\alpha.40$ catalog, and the WISE team and GALEX team for their wonderful released data. We thank Dr.Xianzhong Zheng for given suggestions.

This project is supported by the National Natural Science Foundation of China (Grant Nos. 11403037, 11173030, 11225316, 11503013, 11403061, U1531245, 11303038); This project is also supported by the Strategic Priority Research Program, "The Emergence of Cosmological Structures" of the Chinese Academy of Sciences (Grant No.XDB09000000) and the China Ministry of Science and Technology under the State Key Development Program for Basic Research (Grant Nos. 2012CB821803, 2014CB845705). This work is also sponsored in part by the Chinese Academy of

Sciences (CAS), through a grant to the CAS South America Center for Astronomy (CASSACA) in Santiago, Chile.

The James Clerk Maxwell Telescope is operated by the East Asian Observatory on behalf of the National Astronomical Observatories of China and the Chinese Academy of Sciences, the National Astronomical Observatory of Japan, Academia Sinica Institute of Astronomy and Astrophysics, the Korea Astronomy and Space Science Institute, with additional funding support from the Science and Technology Facilities Council of the United Kingdom and participating universities in the United Kingdom and Canada. Our JCMT project ID is M15BI057

REFERENCES

- Blanton, M. R. & Moustakas, J. 2009, *ARA&A*, 47, 159
- Boissier, S., Gil de Paz, A., & Boselli, A. 2008, *ApJ*, 681, 244
- Bolatto, A. D., Wolfire, M., & Leroy, A. K. 2013, *ARA&A*, 51, 207
- Braine, J., Herpin, F., & Radford, S. J. E. 2000, *A&A*, 358, 494
- Burkholder, V., Impey, C., & Sprayberry, D. 2001, *AJ*, 122, 2318
- Das, M., Boone, F., & Viallefond, F. 2010, *A&A*, 523, A63
- Das, M., Kantharia, N., Ramya, S., Prabhu, T. P., McGaugh, S. S., & Vogel, S. N. 2007, *MNRAS*, 379, 11
- de Blok, W. J. G., McGaugh, S. S., & van der Hulst, J. M. 1996, *MNRAS*, 283, 18
- de Blok, W. J. G. & van der Hulst, J. M. 1998a, *A&A*, 335, 421
- . 1998b, *A&A*, 336, 49
- de Blok, W. J. G., van der Hulst, J. M., & Bothun, G. D. 1995, *MNRAS*, 274, 235
- de Vaucouleurs, G., de Vaucouleurs, A., Corwin, Jr., H. G., Buta, R. J., Paturel, G., & Fouqué, P. 1991, *Third Reference Catalogue of Bright Galaxies. Volume I: Explanations and references. Volume II: Data for galaxies between 0^h and 12^h . Volume III: Data for galaxies between 12^h and 24^h .*
- Donoso, E., Yan, L., Tsai, C., Eisenhardt, P., Stern, D., Assef, R. J., Leisawitz, D., Jarrett, T. H., & Stanford, S. A. 2012, *ApJ*, 748, 80
- Du, W., Wu, H., Lam, M. I., Zhu, Y., Lei, F., & Zhou, Z. 2015, *AJ*, 149, 199
- Epinat, B., Amram, P., & Marcelin, M. 2008, *MNRAS*, 390, 466
- Fan, Z., Wang, H., & Jiang, X. 2016, *ArXiv e-prints*
- Gerritsen, J. P. E. & de Blok, W. J. G. 1999, *A&A*, 342, 655
- Giovanelli, R., Haynes, M. P., & Kent, B. R. 2005, *AJ*, 130, 2598

- Haynes, M. P., Giovanelli, R., & Martin, A. M. 2011, *AJ*, 142, 170
- Hirst, P. & Cavanagh, B. 2005, *Starlink User Note*, 236
- Impey, C. & Bothun, G. 1997, *ARA&A*, 35, 267
- Jiang, X.-J., Wang, Z., Gu, Q., Wang, J., & Zhang, Z.-Y. 2015, *ApJ*, 799, 92
- Jimenez, R., Padoan, P., Matteucci, F., & Heavens, A. F. 1998, *MNRAS*, 299, 123
- Kennicutt, Jr., R. C. 1998, *ARA&A*, 36, 189
- Knezek, P. M. 1993, PhD thesis, Massachusetts Univ., Amherst.
- Lauberts, A. & Valentijn, E. A. 1989, *The surface photometry catalogue of the ESO-Uppsala galaxies*
- Leroy, A. K., Walter, F., & Bigiel, F. 2009, *AJ*, 137, 4670
- Leroy, A. K., Walter, F., & Brinks, E. 2008, *AJ*, 136, 2782
- Matthews, L. D. & Gao, Y. 2001, *ApJ*, 549, L191
- Matthews, L. D., Gao, Y., Uson, J. M., & Combes, F. 2005, *AJ*, 129, 1849
- Matthews, L. D., van Driel, W., & Monnier-Ragaigne, D. 2001, *A&A*, 365, 1
- Matthews, L. D. & Wood, K. 2001, *ApJ*, 548, 150
- McGaugh, S. S. 1994, *ApJ*, 426, 135
- McGaugh, S. S. & Bothun, G. D. 1994, *AJ*, 107, 530
- McGaugh, S. S. & de Blok, W. J. G. 1997, *ApJ*, 481, 689
- Narayanan, D., Krumholz, M. R., Ostriker, E. C., & Hernquist, L. 2012, *MNRAS*, 421, 3127
- O’Neil, K., Bothun, G., van Driel, W., & Monnier Ragaigne, D. 2004, *A&A*, 428, 823
- O’Neil, K., Hofner, P., & Schinnerer, E. 2000, *ApJ*, 545, L99

- O’Neil, K., Schinnerer, E., & Hofner, P. 2003, *ApJ*, 588, 230
- Peebles, P. J. E. 2001, *ApJ*, 557, 495
- Pickering, T. E., Impey, C. D., van Gorkom, J. H., & Bothun, G. D. 1997, *AJ*, 114, 1858
- Pustilnik, S. A., Martin, J.-M., Tepliakova, A. L., & Kniazev, A. Y. 2011, *MNRAS*, 417, 1335
- Savage, B. D. & Mathis, J. S. 1979, *ARA&A*, 17, 73
- Schombert, J. 1998, *AJ*, 116, 1650
- Schombert, J. M., Bothun, G. D., Impey, C. D., & Mundy, L. G. 1990, *AJ*, 100, 1523
- Schruba, A., Leroy, A. K., & Walter, F. 2012, *AJ*, 143, 138
- Shetty, R., Glover, S. C., Dullemond, C. P., & Klessen, R. S. 2011, *MNRAS*, 412, 1686
- Subramanian, S., Ramya, S., Das, M., George, K., Sivarani, T., & Prabhu, T. P. 2016, *MNRAS*, 455, 3148
- van der Hulst, J. M., Skillman, E. D., Smith, T. R., Bothun, G. D., McGaugh, S. S., & de Blok, W. J. G. 1993, *AJ*, 106, 548
- van Zee, L. 2000, *AJ*, 119, 2757
- Wen, X.-Q., Wu, H., & Zhu, Y.-N. 2013, *MNRAS*, 433, 2946
- Wolfire, M. G., Hollenbach, D., & McKee, C. F. 2010, *ApJ*, 716, 1191
- Wu, H., Burstein, D., & Deng, Z. 2002, *AJ*, 123, 1364
- Wyder, T. K., Martin, D. C., & Barlow, T. A. 2009, *ApJ*, 696, 1834
- Young, J. S. & Knezek, P. M. 1989, *ApJ*, 347, L55
- Zheng, Z., Shang, Z., & Su, H. 1999, *AJ*, 117, 2757

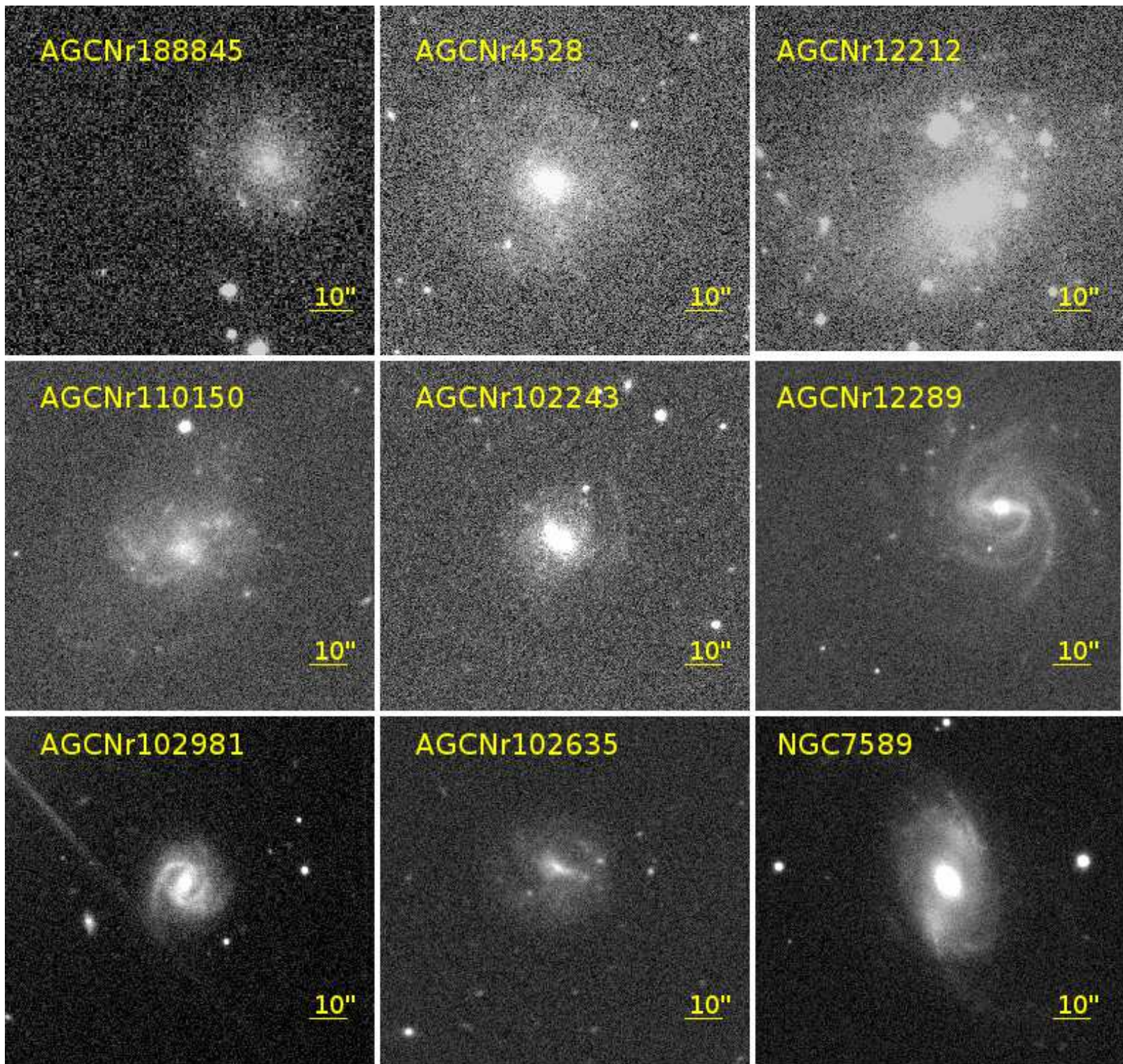


Fig. 1.—: SDSS r band images of our LSBGs.

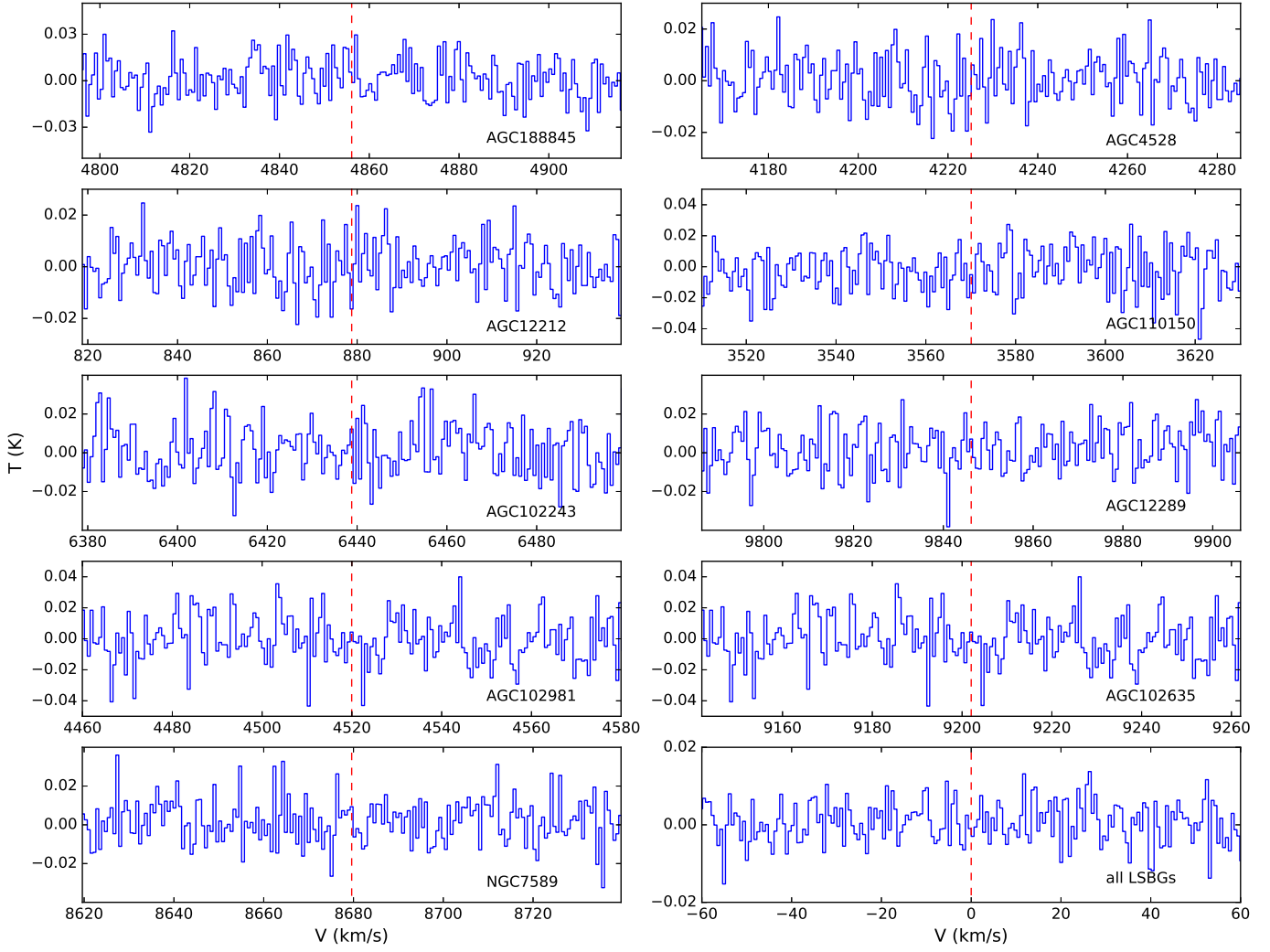


Fig. 2.—: Nine individual and combined CO(J=2-1) spectra of LSBGs. The red dashed line mark the position of emission line of redshifted CO(J=2-1).

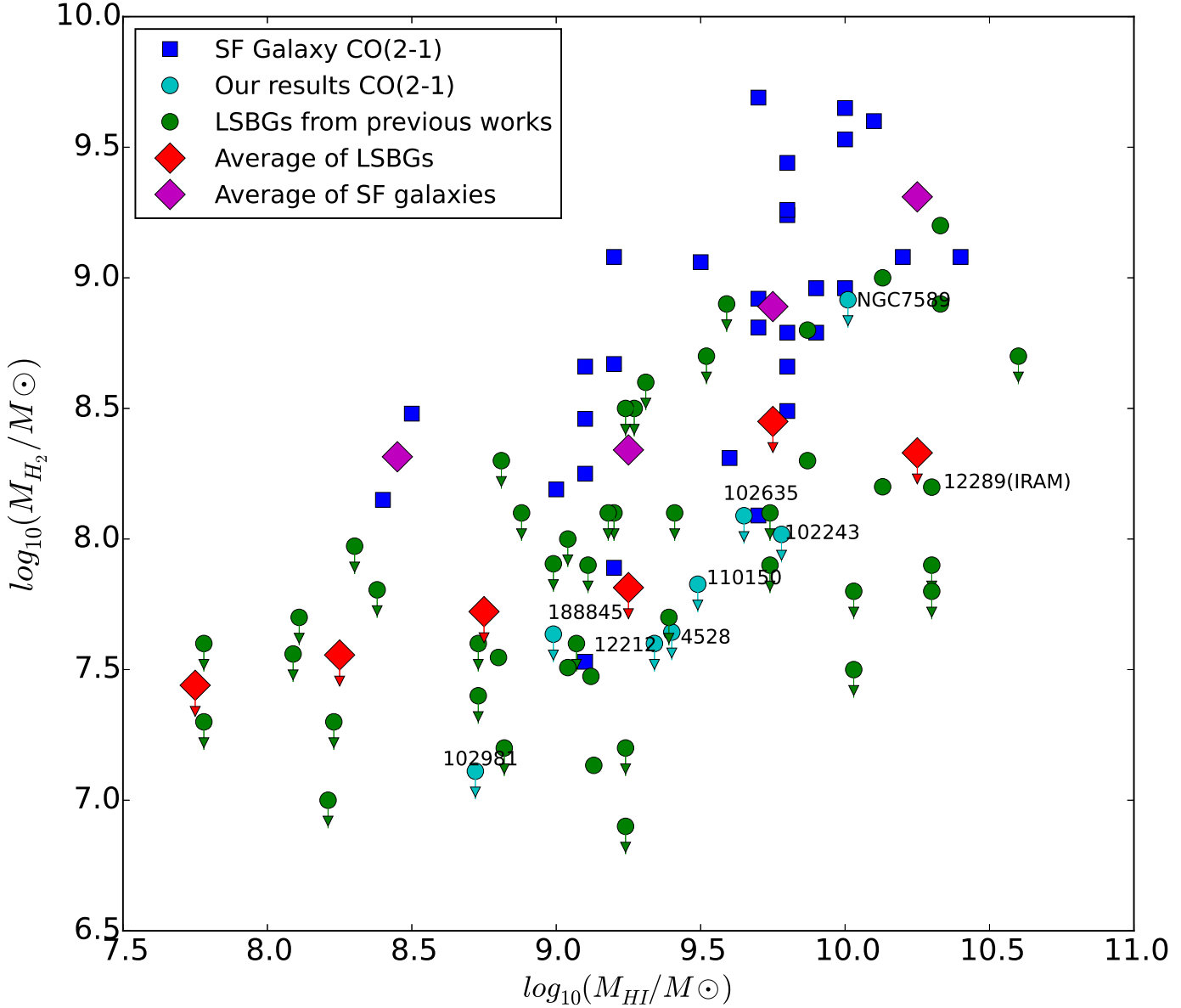


Fig. 3.—: HI mass vs. H₂ mass. The cyan dots are LSBGs from this survey, the green dots are LSBGs from previous works (Schombert et al. 1990; de Blok & van der Hulst 1998a; O’Neil et al. 2000; Braine et al. 2000; O’Neil et al. 2003). Blue squares are SF galaxies from Jiang et al. (2015). The red and purple diamonds present the average molecular mass of LSBGs and SF galaxies, respectively. The arrows indicate the upper limits.

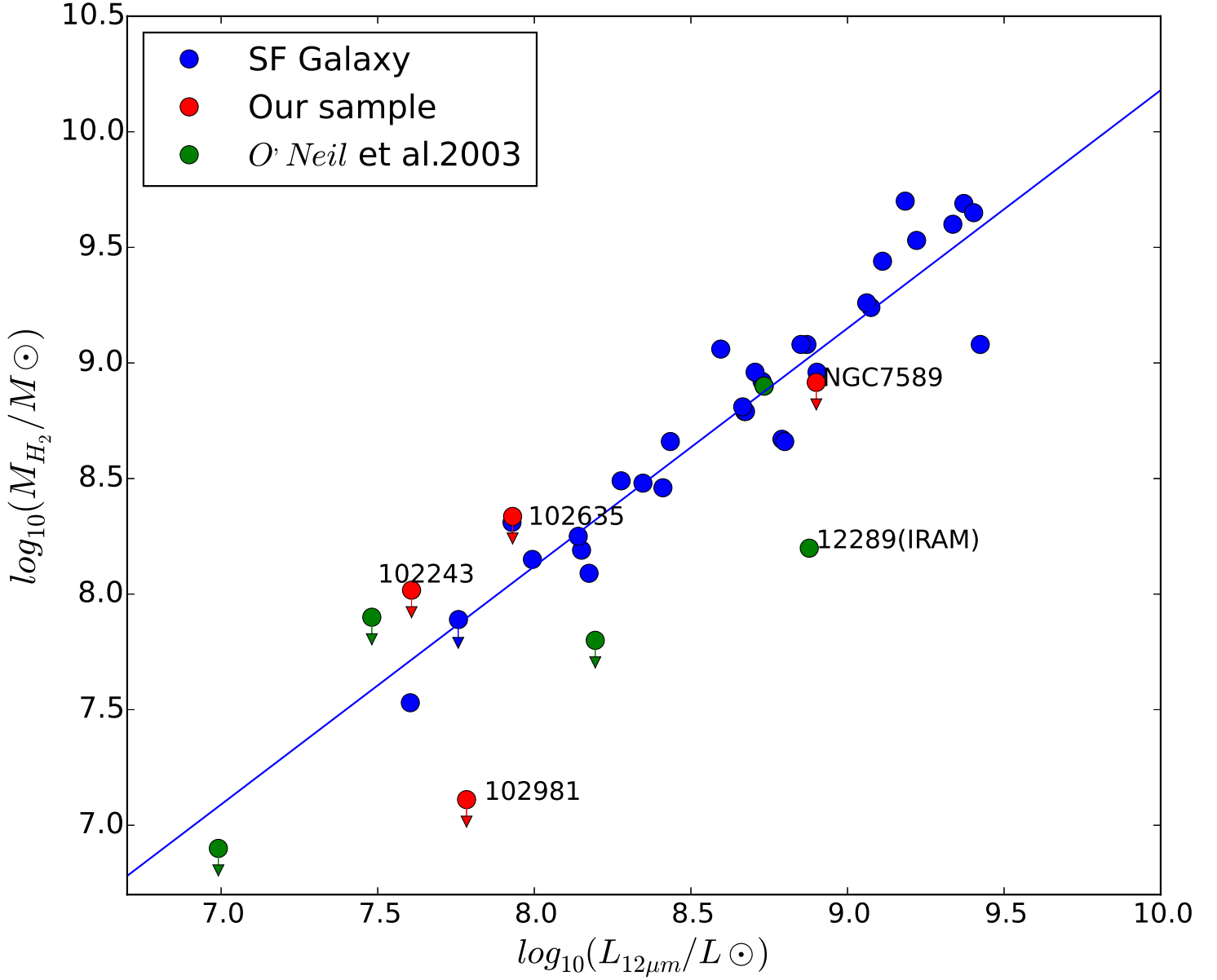


Fig. 4.—: Luminosity of $12\mu m$ vs. M_{H_2} . The red dots are LSBGs from this work, green dots are from O’Neil et al. (2003) and the blue dots are SF galaxies from Jiang et al. (2015). The arrows indicate the upper limits.

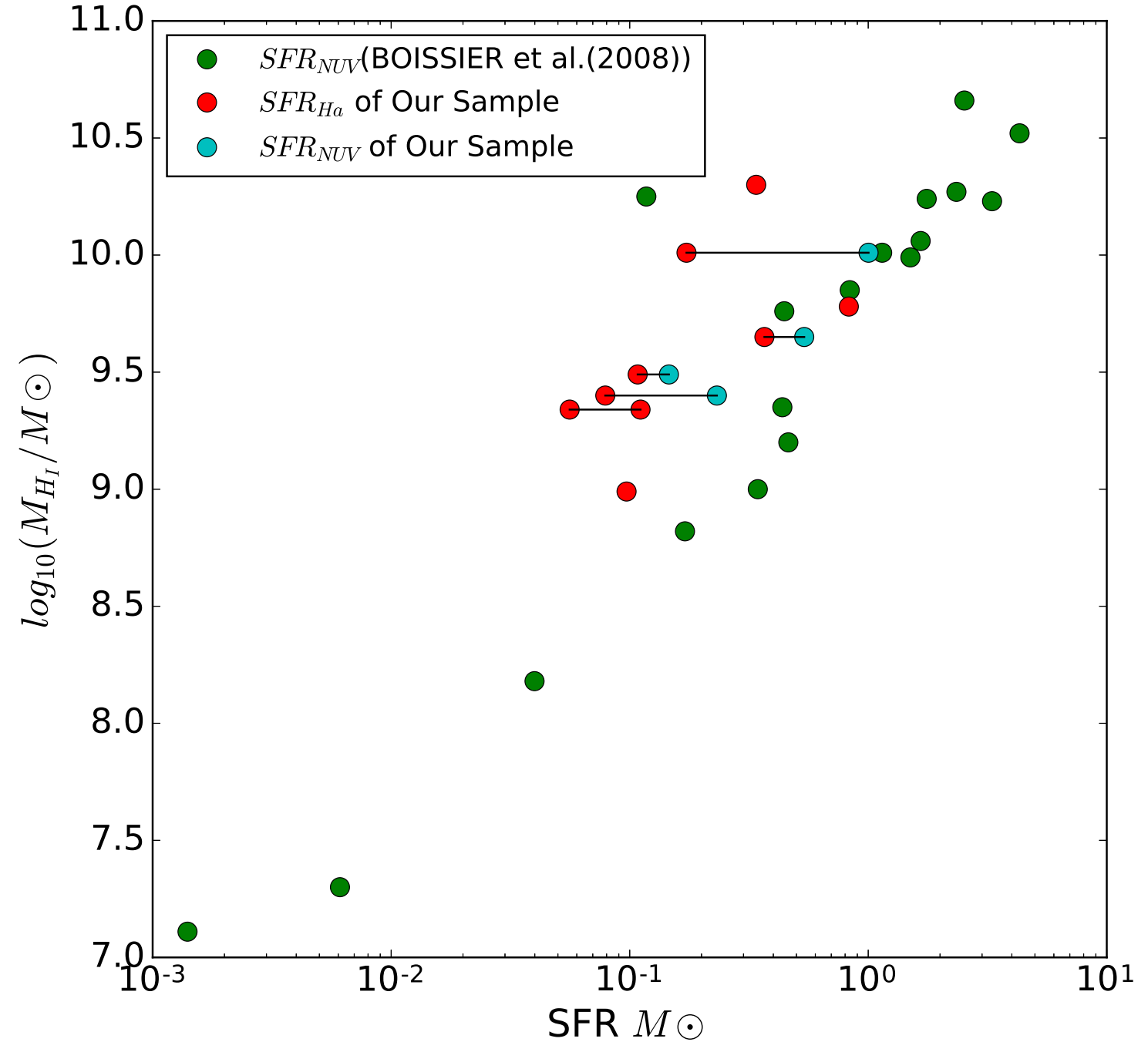


Fig. 5.—: HI mass vs. SFR. The red dots are SFR calculated by $H\alpha$ and the blue dots are SFR calculated by NUV luminosity. The black line connects the same target. The green dots are the sample of LSBGs from Boissier et al. (2008).

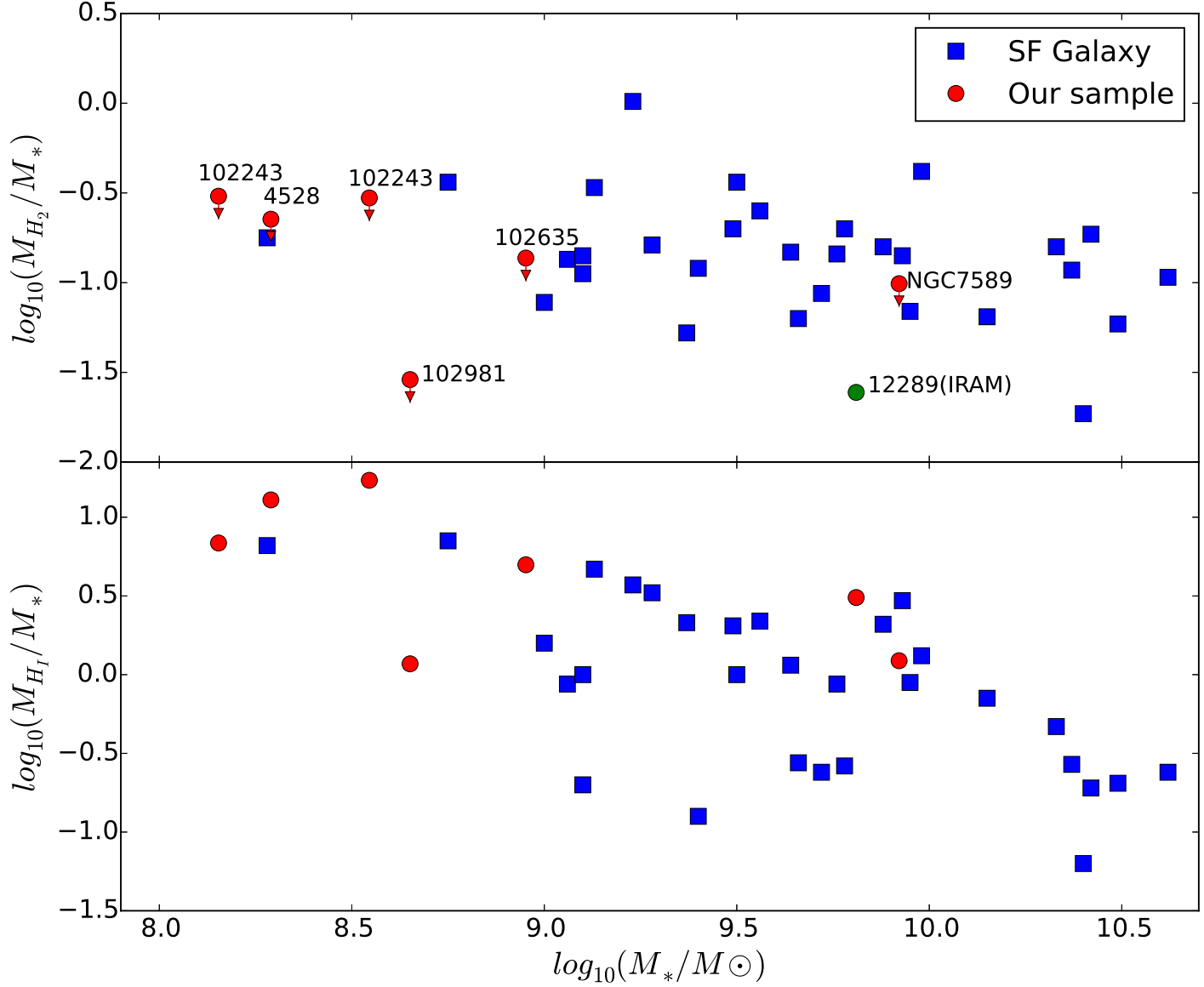


Fig. 6.— Stellar mass (M_*) vs. the ratio of M_{H_2}/M_* (upper) and M_{HI}/M_* (lower). The red dots are LSBGs from this work and the blue squares are SF galaxies (Jiang et al. 2015). The arrows indicate the upper limits.

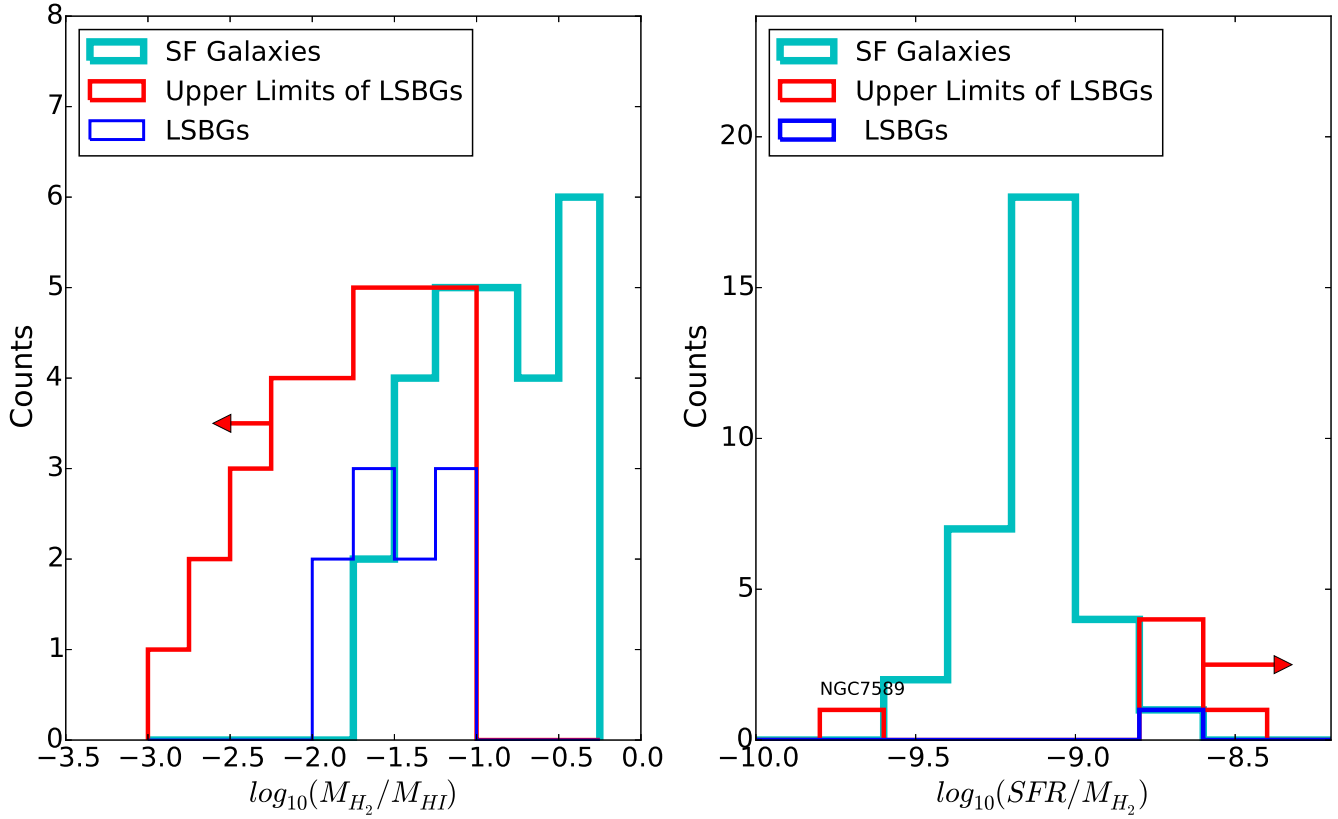


Fig. 7.—: Left panel: The distribution of M_{H_2}/M_{HI} . Right panel: The distribution of SFR/M_{H_2} . The red histogram represents upper limits of LSBGs and the blue histogram represents those detected molecular LSBGs. All LSBGs data are from our sample and previous works(Schombert et al. 1990; de Blok & van der Hulst 1998a; O’Neil et al. 2000; Braine et al. 2000; O’Neil et al. 2003). The cyan histogram represents SF galaxies(Jiang et al. 2015). The arrows means upper limits.

Table 1. Parameters of Low Surface brightness Galaxies

Name	RA(J2000)	Dec(J2000)	V_{HeI} kms ⁻¹	$u_{B(0)obs}$ mag arcsec ⁻²	W_{50}^a kms ⁻¹	$\log M_{HI}$ M _⊙	D Mpc	Major-axis arcsec	z	NUV _{AB} mag	r _{SDSS} mag	W1 ^b mag	W3 ^c mag
AGCNR188845	08:01:13.02	+11:37:24.48	4935	23.056	79	8.99	72.5	54	0.0164		16.30 ±0.02	13.923 ±0.044	
AGCNR4528	08:40:58.60	+16:11:00.14	4288	22.900	88	9.40	63.6	66	0.0143	17.56 ±0.02	15.90 ±0.01	13.335 ±0.028	
AGCNR12212	22:50:30.26	+29:08:19.52	894	23.040	99	9.34	24.3	62	0.0029		15.02 ±0.00		
AGCNR110150	01:14:45.56	+27:08:11.10	3617	22.760	108	9.49	49.5	80	0.0120	17.52 ±0.03	16.01 ±0.01		
AGCNR102243	00:05:05.06	+23:58:14.09	6575	22.500	139	9.78	89.0	52	0.0219		20.59 ±0.04	13.494 ±0.019	10.83 ±0.336
AGCNR12289	22:59:41.52	+24:04:29.77	10165	22.650	217	10.3	140.2	35	0.0339		14.60 ±0.00	11.658 ^{ct} ±0.007	8.64 ±0.034
AGCNR102981	00:02:55.56	+28:16:38.78	4583	22.540	65	8.72	66.2	46	0.0152		15.41 ±0.00	12.615 ±0.012	9.74 ±0.117
AGCNR102635	00:16:12.22	+24:50:59.04	9491	22.573	94	9.65	138.7	46	0.0316	18.34 ±0.04	16.66 ±0.01	13.551 ±0.026	10.98 ±0.261
NGC7589	23:18:15.60	+00:15:40.00	8938	25.000 ^d	345	10.01	120.7	76	0.0298	17.53 ±0.01	14.08 ±0.00	11.084 ±0.009	8.26 ±0.024

^a W_{50} is the Full Width at Half Maximum(FWHM) of HI emission line.

^bW1 is 3.4 μ m band of the WISE.

^cW3 is 12 μ m band of the WISE.

^dFor NGC 7589, its surface brightness is from de Vaucouleurs et al. (1991).

Table 2. Observation Details

Name	Receiver	Weather band	Frequency GHZ	Integration time hour	rms noise mk	Facility	H α filter ^a Å	Exp _{Hα} s	Exp _{Rαband} s
AGCNR188845	RxA3/JCMT	4	226.91	1.63	2.7	BFOSC/2.16	6660.0	1800	600
AGCNR4528	RxA3/JCMT	4	227.29	2.62	2.0	BFOSC/2.16	6660.0	1800	600
AGCNR12212	RxA3/JCMT	5	229.86	7.8	2.1				
AGCNR110150	RxA3/JCMT	5	227.67	7.4	2.8	BFOSC/2.16	6660.0	1800	600
AGCNR102243	RxA3/JCMT	5	225.60	7.8	2.6	BFOSC/2.16	6710.0	1800	600
AGCNR12289	RxA3/JCMT	5	222.99	7.6	3.3	BFOSC/2.16	6760.0	1800	600
AGCNR102981	RxA3/JCMT	5	227.06	7.8	2.0	BFOSC/2.16	6660.0	1800	600
AGCNR102635	RxA3/JCMT	5	223.47	8.3	3.1	BFOSC/2.16	6760.0	1800	600
NGC7589	RxA3/JCMT	5	223.87	7.8	2.1				

^aThe central wavelength of H α filter.

Table 3. Upper limits of H₂ masses in the beam size

Name	SFR _{Hα} M _⊙ yr ⁻¹	log(SFE) _{Hα} yr ⁻¹	SFR _{NUV} M _⊙ yr ⁻¹	log(SFE) _{NUV} yr ⁻¹	logL _{CO} Kkms ⁻¹ pc ²	Beam Filling Factor	logM _{H₂Total} M _⊙	M _{H₂Total} /M _{HI}	logL _{3.4} L _⊙	logM _* M _⊙
AGCNR188845	0.097	-10.012			<6.71	1.35	<7.635	<0.044	7.316	8.154
AGCNR4528	0.079	-10.500	0.232	-10.037	<6.50	1.65	<7.643	<0.017	7.437	8.290
AGCNR12212 ^{*a}	0.111	-10.300			<5.747	1.55	<7.612	<0.0201		
	0.056	-10.599								
AGCNR110150	0.108	-10.457	0.146	-10.327	<6.52	2.07	<7.827	<0.022		
AGCNR102243	0.829	-9.865			<7.10	1.35	<8.017	<0.017	7.665	8.545
AGCNR12289 ^{*b}	0.339	-10.776			<7.79	1.00	<8.615	<0.020	8.795	9.810
AGCNR102981 ^{*c}	NAN				<6.411	1.76	<7.07	<0.018	7.760	8.651
AGCNR102635	0.367	-10.085	0.539	-9.930	<7.39	1.76	<8.336	<0.048	8.029	8.952
NGC7589 ^{*d}	0.173	-10.782	1.003	-10.018	<7.66	1.90	<8.960	<0.0806	8.894	9.922

^aFor AGCNR12212, the two different SFR_{H α} results are from the works(van Zee 2000; Epinat et al. 2008). We did not derive its H α flux from our observation.

^bThis just is the result with the observations of JCMT. The CO content of AGCNR12289 had been detected by O'Neil et al. (2003) with the IRAM and the ratio of M_{H₂}/M_{HI} is 0.008.

^cFor AGCNR102981, we did not derive its H α flux from our observation.

^dFor NGC 7589, the SFR_{H α} is calculated by SDSS spectra (Subramanian et al. 2016).